3D Lattice Model for Post-Yield and Fracture Behaviour of Timber

Thomas REICHERT
Research Student
Centre for Timber Engineering, Napier University
Edinburgh, UK

Dr Daniel RIDLEY-ELLIS
Principal Research Fellow
Centre for Timber Engineering, Napier University
Edinburgh, UK

Summary

The paper describes the development of a bespoke Finite Element program to model timber with a three dimensional lattice of single spring elements. These springs mimic meso-scale timber behaviour, namely the crushing and separation of fibre bunches by following a tri-linear load-displacement curve. Strength and stiffness parameters for longitudinal, lateral and diagonal elements are randomised for heterogeneity. To save computing time, two specialised algorithms have been implemented to perform a nonlinear analysis faster than an iterative Newton-Raphson algorithm. The algorithms have been adopted and extended to suit a 3D lattice model for timber. Furthermore lattice elements have only been used in areas where plasticity and fracture is expected, with transverse isotropic continuum elements elsewhere. The general calibration procedure of this hybrid model to tested timber specimens of Sitka spruce (*Picea sitchensis*) is described.

1. Concept Lattice Model

Lattice models have been used widely for concrete, but have only recently been applied to timber, e.g. [1][2][3]. A clear advantage of modelling timber with a lattice is the possibility to predict brittle failure without prior knowledge of the failure location and therefore with no need for re-meshing the Finite Element (FE) model.

The basic unit cell in a lattice has to be constructed to be periodically repeating in space (Fig. 1). In this lattice, each cell consists of six different types of elements. Longitudinally orientated springs transfer load in the X direction (grain direction) and lateral springs in the Y and Z direction. Diagonal springs resist shear in the XY, XZ and YZ plane, as well as providing additional X, Y and Z components. This can be simplified by the assumption of transverse isotropy, to four independent elements by equating the Y and the Z direction. Thus, elements in the XY plane are the same as

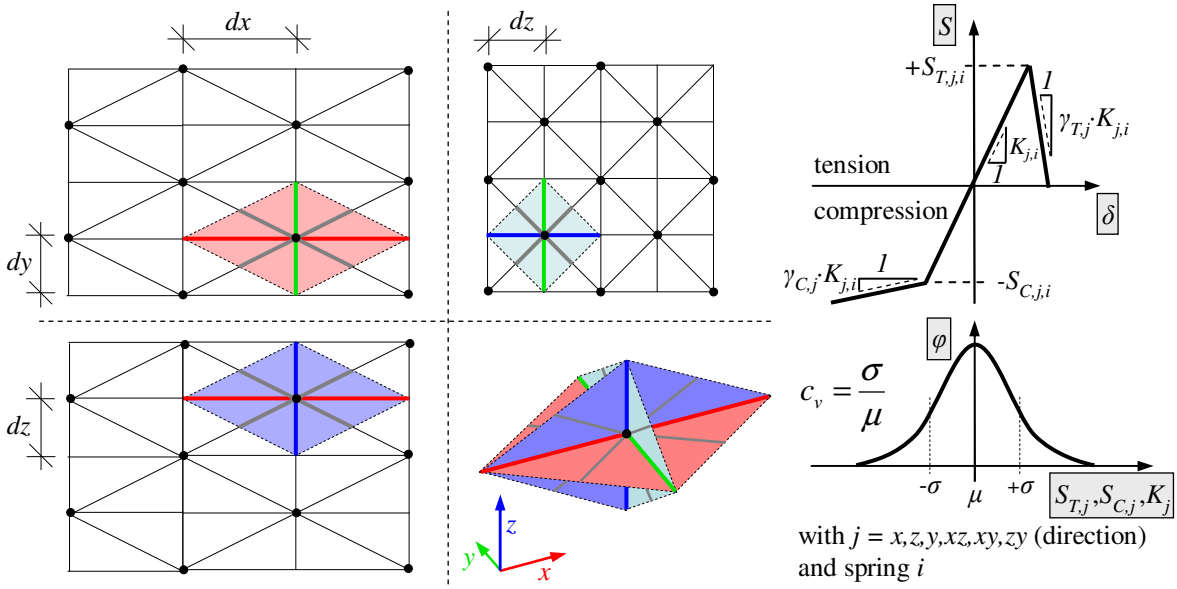

Fig. 1 Lattice structure with longitudinal (red), lateral (green/blue) and diagonal (grey) "half" springs in one unit cell (left), load-displacement curve for spring i (top, right) and a definition of c_v with mean and standard deviation (bottom, right)

their respective elements in the XZ plane. A complete nomenclature can be found at the end of this paper.

In order to create a lattice with as few nodes as possible, they have been arranged in a diagonal checked pattern. Thus, instead of constructing nodes at each potential junction of springs only every second one is used. Each element follows a tri-linear load-displacement curve with limit strength and yield strength values respectively under tension and compression, followed by a softening or fracture line.

Material heterogeneity can be implemented by assigning randomised strength ($S_{C,j}$ and $S_{T,j}$) and stiffness (K_j) properties to springs based on a mean value for each spring type j (x, y/z, xy/xz and yz) and a coefficient of variation (c_v). This coefficient is assumed to be 0.2 since it has only minor influence on the bulk model behaviour [2]. The growth rings can be taken into account as structured variation of properties in the lattice. This is implemented by mapping generated growth rings on the lattice and changing the mean strength and stiffness properties of lattice members according to their assumed position within these rings (section 1.2).

1.1 Nonlinear Solution

Former lattice models for timber, e.g. [1][2][3], adopted a simple technique to solve for the nonlinear solution: After assembling the global stiffness matrix, this system of equations is solved for a fixed displacement step. The resulting stress for each element is computed and checked if it exceeds its predefined maximum strength. Elements are removed accordingly and the process is repeated until no element fails. Then the next displacement is assigned. This algorithm is repeated until the final displacement step assigned or the system becomes singular. However, with this technique any accumulated elastic work stored in the lattice before breaking occurs is neglected. Since the model described in this paper will be used to perform contact and geometric nonlinear analysis in the future, the solution algorithm required a more general approach, as for example the Newton-Raphson algorithm.

To further save computation time, a specialised technique [4] has been adopted. Jirásek and Bažant call it the "Method of Inelastic Forces" (MIF) and the "Step Size Control" (SSC) algorithm. The latter allows for faster computation by following the solution path through single linear steps from one element changing its stiffness to the next element changing. Thus, no additional iteration is necessary. Further, the MIF treats any change that would occur in the matrix due to a change in the element's stiffness, as an added inelastic force that represents the difference between the system with changed stiffness and the elastic one. Thus, only the force vector has to be modified and it is not necessary to solve the global stiffness matrix again. The interested reader is referred to a more detailed description of this algorithm in the original paper [4]. For this research, the SSC method has been modified to allow for a tri-linear load-displacement definition of the spring elements as depicted in Fig. 1.

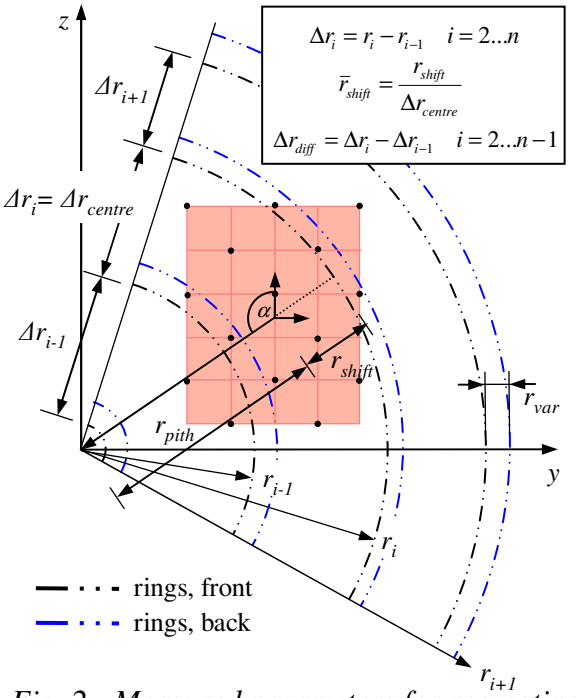

Fig. 2 Measured parameters for recreating a growth ring structure in the model

1.2 Structured Heterogeneity

Heterogeneity, on the level of the growth ring structure, is mapped on a lattice of the cell size of 2 x 1 x 1 mm (dx x dy x dz). This size results from a balance between acceptable computational effort for larger lattices and represented detail of the growth ring structure. The mean ring width measured from test specimens has been 5.47 mm, with a c_v of 24.8%. Specimens with ring width less than 2 mm were discarded. This ensures that one growth ring encompasses at least two lattice cells.

Several measurements were taken from the tested specimens. The cross section of each one (front and back) was scanned with an ordinary flatbed

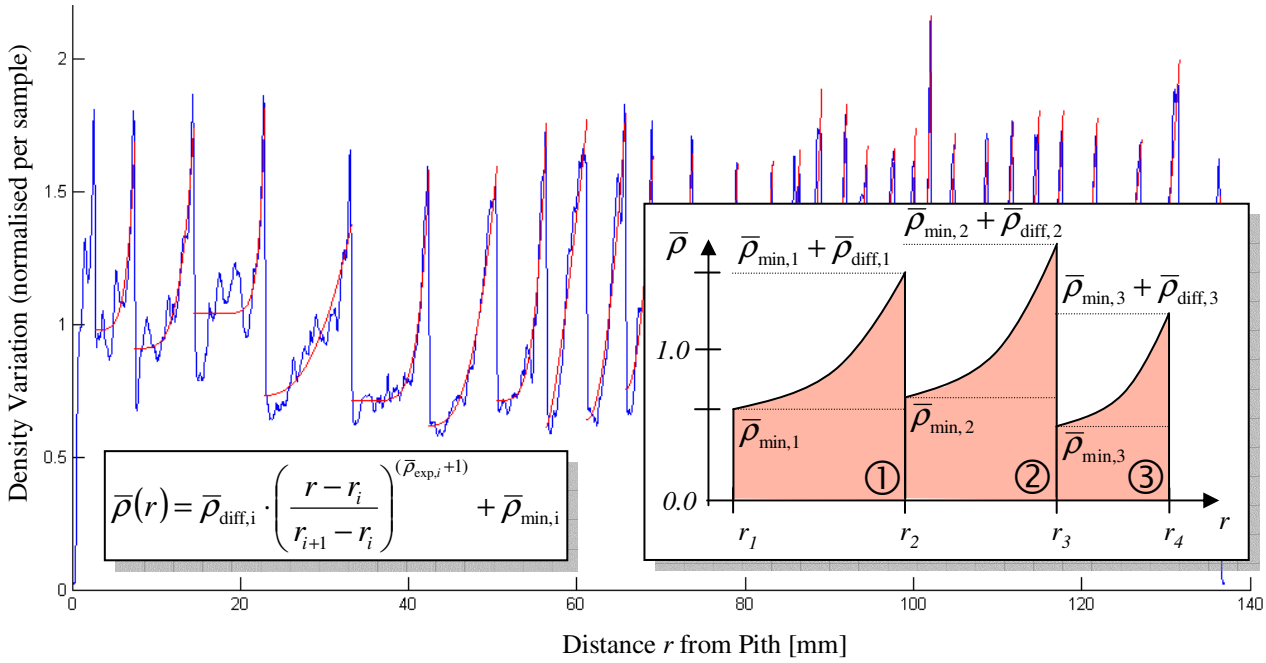

Fig. 3 Density profile with fitted curve of power functions in each growth ring

scanner. A programme was written that enables the user to draw 3-point circles onto the latewood of each growth ring in these images. By averaging the centre points of each circle, the assumed position of the pith can be determined. With this information the following parameters can be obtained from one specimen (Fig. 2): α, r_{pith}, $\bar{r}_{shift}$, *mean* Δr_{diff} and *mean* r_{var}.

Mean values are calculated along with their coefficients of variation from the specimens of one test series. This serves then as input parameters to create a random ring structure for the lattice model, based on the characteristics of tested specimens.

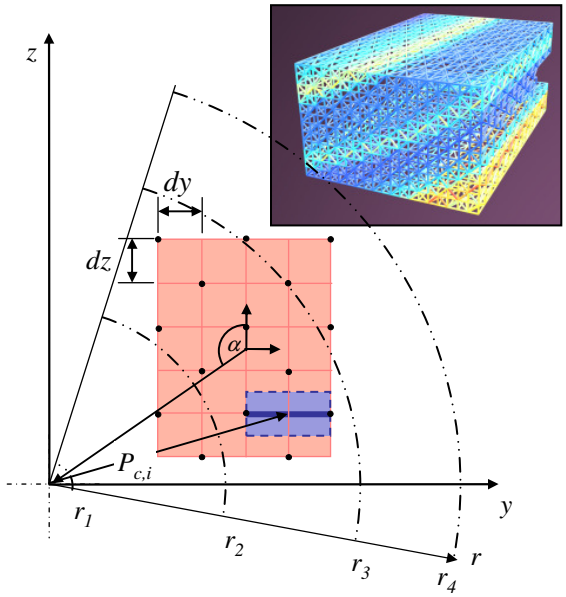

Fig. 4 Density profile mapped on lattice

1.3 Mapping the Density Profile

In order to map the ring structure on the lattice, the simplest assumption would be to correlate stiffness and strength variation directly with density variation within a growth ring. Therefore, density measurements from Sitka spruce samples were taken and have been normalised. The experimental work was done by the chemistry department in the University of Glasgow, which used an Itrax density scanner [7]. Fig. 3 shows a density profile for one radial strip, plotted from pith to bark (blue line). Each peak represents the end of one growth ring. A good approximation of these lines is a fitted power function curve (red line) that encompasses one growth ring from one peak to the next one. The equation for these approximated curves is given in the left box of Fig. 4. The right box depicts the resulting curve for this equation for three rings. From several of these radial specimens mean values of $\bar{\rho}_{min,i}$, $\bar{\rho}_{diff,i}$, $\bar{\rho}_{\exp,i}$ and their c_v can be calculated, serving as further input parameters to generate a density profile for the model.

Each individual *full* spring encompasses an area of the cross section of $dy \cdot dz$ for longitudinal and diagonal springs and $2 \cdot dy \cdot dz$ for lateral springs, as shown in Fig. 4. The average normalised density of this area from a randomly generated profile is calculated. Finally, the mean strength and stiffness parameters for this particular spring are simply adjusted by multiplying this value with the original mean parameters.

2. Methodology

As shown in the load-displacement curve definition of one spring *i* in Fig. 1, three types of mean parameters have to be adjusted: firstly, the mean stiffness values K that can be directly (with limitations) derived from E-moduli, secondly, the mean strength parameters S_C and S_T for each spring type that will be determined by trial and error, and thirdly, the parameters γ_T and γ_C that define the softening curve.

All tested specimens came from one timber species, Sitka spruce (*Picea sitchensis*).

Given that the timber behaves transverse isotropic on the small scale that it is modelled, it can be assumed that parameters in the Y and Z direction are the same. Thus, in summary, there are four independent mean elastic parameters (K_x, $K_y = K_z$, K_{yz}, $K_{xz} = K_{xy}$, K_{yz}), six independent mean strength parameters ($S_{C,x}$, $S_{T,x}$, $S_{C,y} = S_{C,z}$, $S_{T,y} = S_{T,z}$, $S_{CT,xy} = S_{CT,xz}$, $S_{CT,yz}$) and two softening stiffness parameters in compression ($\gamma_{C,x}$ and $\gamma_{C,y} = \gamma_{C,z}$). The remaining represent a very steep softening curve, thus ($\gamma_{T,x} = \gamma_{T,y} = \gamma_{T,z} = \gamma_{CT,xy} = \gamma_{CT,xz} = \gamma_{CT,yz} \approx -\infty$).

While the stiffness parameters can be obtained from given E-moduli, the strength parameters are adjusted by means of comparisons between tested small clear specimens under various loading conditions and their respective FE models. Fig. 5 demonstrates the methodology of the calibration.

2.1 Elastic Parameters

The K values for a lattice can not be adjusted entirely freely to represent full anisotropic or simply transverse isotropic behaviour. The geometry imposes certain limitations. These could be overcome by introducing angular springs that act in between the existing springs in one unit cell. With this, it would be possible to adjust, for example, the elastic stiffness K_x and K_z independently from the shear modulus G_{xz}.

However, this has not been done for this research as it adds considerably to the computational problem. In this model (without angular springs), calculating the possible elastic parameters from the independent spring stiffness of a lattice cell can be performed according to [5] and shall be presented here briefly. This can be achieved by equating strain energy stored in a unit lattice cell and energy stored in the respective continuum of the same volume.

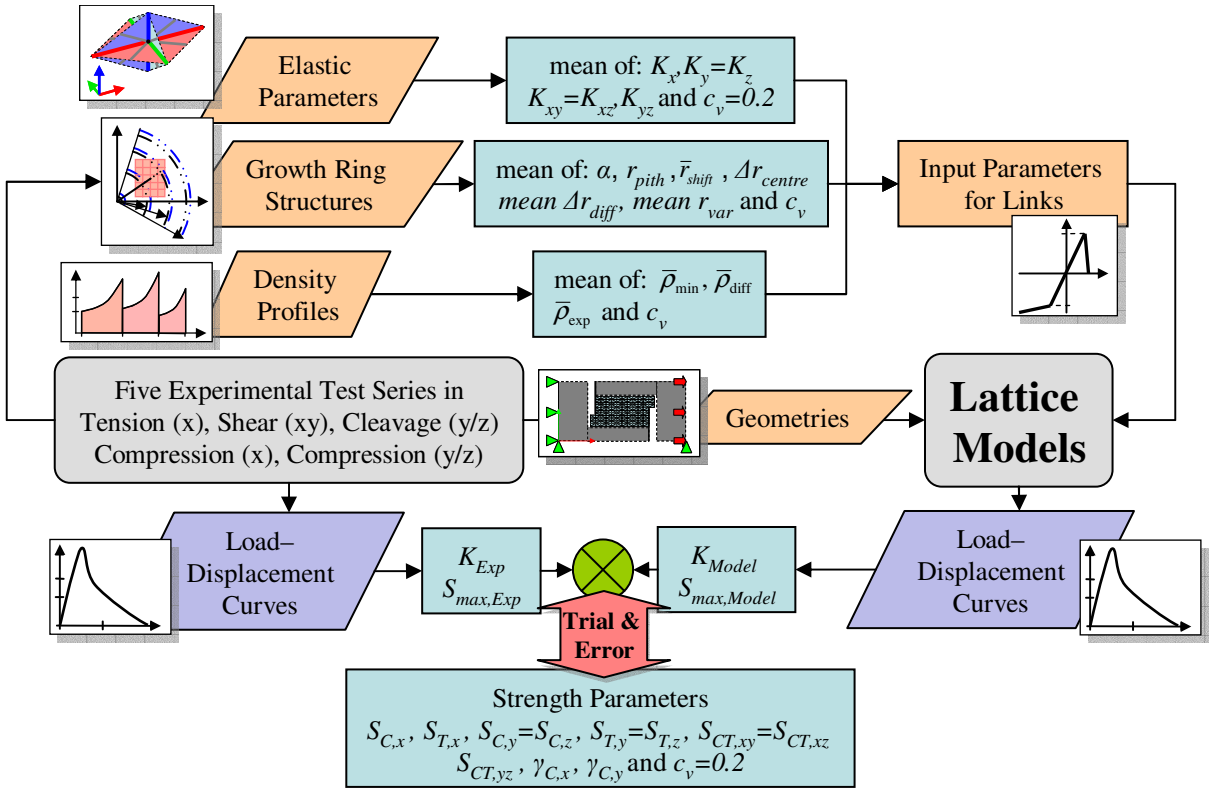

Fig. 5 Flowchart for the calibration process

$$U_{cell} = U_{continuum} \tag{1}$$

The strain energy can further be written as:

$$U_{cell} = \sum_b \frac{1}{2} E_b = \frac{1}{2} \sum_b^{N_b} (F \cdot u)^{(b)} \quad U_{continuum} = \frac{1}{2} \int_V \sigma \cdot \varepsilon dV \tag{2}$$

The former can be arranged as:

$$U_{cell} = \frac{1}{2} \sum_b^{N_b} (Ku \cdot u)^{(b)} \quad U_{continuum} = \frac{1}{2} \varepsilon \cdot C \cdot \varepsilon \tag{3}$$

A subsequent step involves equating both strain energies and connecting displacement u with strain ε, thus deriving the stiffness tensor C. At the final stage C can be written as:

$$C_{ijkm} = \frac{1}{V} \sum_b^{N_b} l^{(b)^2} \cdot K^{(b)} \cdot n_i^{(b)} n_j^{(b)} n_k^{(b)} n_m^{(b)} \qquad i, j, k, m = 1..3 \tag{4}$$

V represents the volume of the unit cell repeating in space ($V=2 \cdot dx \cdot dy \cdot dz$). The resulting stiffness tensor C_{ijkm} of the size 3x3x3x3 can be transferred due to symmetry to the more widely used Voigt Notation with C_{ij} of the size 6x6. From this, the E-moduli and Poisson coefficients can be directly obtained by calculating the inverse C^{-1}. Thus, it is possible to calculate the elastic constants from assumed spring stiffness. However, as mentioned before, due to the geometry of the lattice only limited elastic moduli can be obtained with certain Ks. Therefore, a program was written that optimises the K values to find relatively close E-moduli and Poisson coefficient predictions.

As input values, the E-modulus in the longitudinal direction was measured from tension test data (E_x = 9792 N/mm²). The remaining E-moduli and Poisson ratios were then determined with ratios taken from the Wood Handbook [6]. Since it is assumed that the material behaves transverse isotropic on the small scale of the lattice cells, several elastic parameters are the same. For these instances the mean value is taken as shown in Table 1.

The best fit was achieved by optimising a target function, which is the sum of squared, normalised differences between the calculated elastic parameter and the target parameter (E-modulus, shear-modulus and Poisson ratio). The optimisation routine resulted in the following parameters.

Table 1 Determination of elastic parameters

Elastic Continuum Parameters	Target [N/mm²], [-]	Result [N/mm²], [-]
E_x	9792	9608
$E_y = E_z$	592	681
$G_{xy} = G_{xz}$	612	557
G_{yz}	*not fitted to*	325
$\nu_{xy} = \nu_{xz}$	0.43	0.4862
$\nu_{yz} = \nu_{zy}$	0.34	0.3719
$\nu_{yx} = \nu_{zx}$	*not fitted to*	0.0345
fit Φ_K		0.0635

Lattice Stiffness Parameters	Result [N/mm]
K_x	1423.5
$K_y = K_z$	357.3
$K_{xy} = K_{xz}$	1392.2
K_{yz}	1297.9

Using these resulting K values for the lattice and resulting E, G, ν for solid elements, which adjoin the latter, they will both behave in the same way as far as bulk elastic properties are concerned

2.2 Strength Parameters

Five different calibration tests have been undertaken to obtain load-displacement data for simple stress states: a tensile, shear and cleavage test along with compression tests in the longitudinal and lateral direction. These results serve as an input to calibrate the lattice's strength parameters.

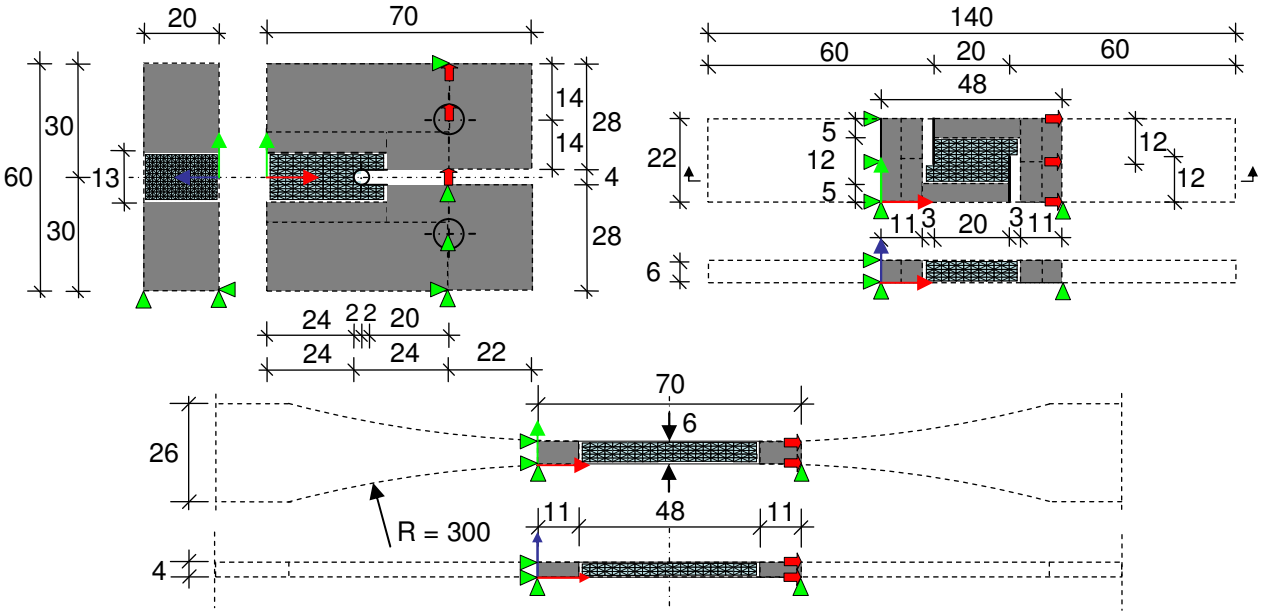

Fig. 6 Model depiction of three test arrangements (from the top left): cleavage (y/z), shear (xy) and tension (x). Note that only part of the specimen is modelled with a lattice, for the remainder transverse isotropic elastic solid elements are used (grey area)

The first three of these types of tests shall be presented here. A depiction of the respective test specimens and FE models is shown in Fig. 6. The red arrows and green triangles represent the applied forces and boundary conditions respectively.

2.3 Program Output

As one of the postprocessor's features, the FE program generates output files in form of 3D surfaces. Individual layers of geometric data of the deformed model as e.g. the lattice elements, solid elements and boundary conditions can be exported. These surfaces can be visualised with a rendering program (e.g. Bryce). To picture the fracture path the FE program generates surfaces (two for each plane in the *xy*, *xz* and *yz*-direction due to the shifted cell arrangement) with different shades of red according to the amount of broken links that this surface encompasses, see Fig. 7.

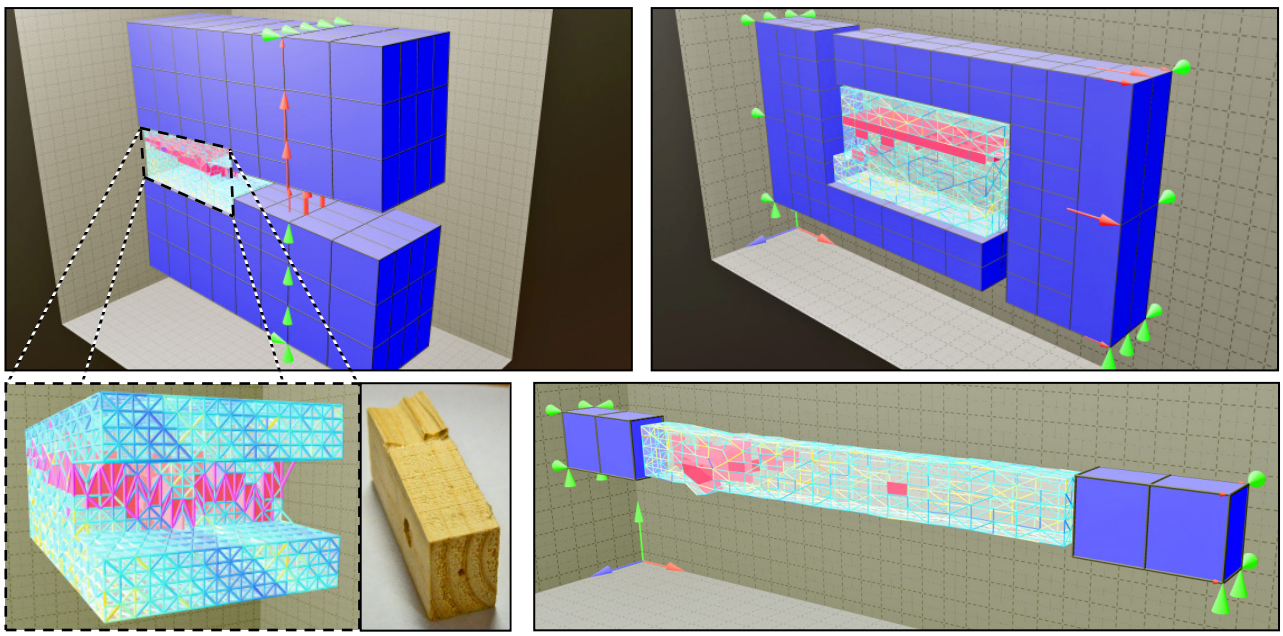

Fig. 7 Model depiction of a cleavage, shear and tension test, lattice colour represents variation in elastic and strength properties, influence of growth ring structure on fracture path for model and tests pictured (bottom, left)

3. Preliminary Results

After a preliminary adjustment of the strength parameters $S_{T,x}$, $S_{T,y/z}$, $S_{CT,xy/xz}$, load-displacement graphs can be obtained. They are plotted in Fig. 8, along with a box plot of the stiffness and maximum load of the model and experimental tests. Similar maximum loads are observed among model and experimental results for all three loading conditions and can be fine-tuned further.

However, predicted and measured stiffness, due to the inherent limitation of the lattice cells to fully model the ratios of elastic properties, show less agreement. Furthermore, post peak behaviour in the experimental shear tests was more pronounced than the model's prediction, which after a short plastic deformation shows brittle fracture. This probably stems from the wide meshed lattice that is used for these relative small shear specimens. Since the model allows adjustment of the softening curve of a spring ($\gamma_{T,j}$), this could serve to be another parameter to adjust for bulk post peak behaviour. However, cleavage models, using a denser mesh, showed better agreement in this regard.

Variation in the system's properties was in all cases predicted to be smaller than observed ones. As an initial assumption for these models, the density was mapped directly without any factor on the lattice's properties. Better model predictions might be obtained by applying a factor to the density variation for specific spring types.

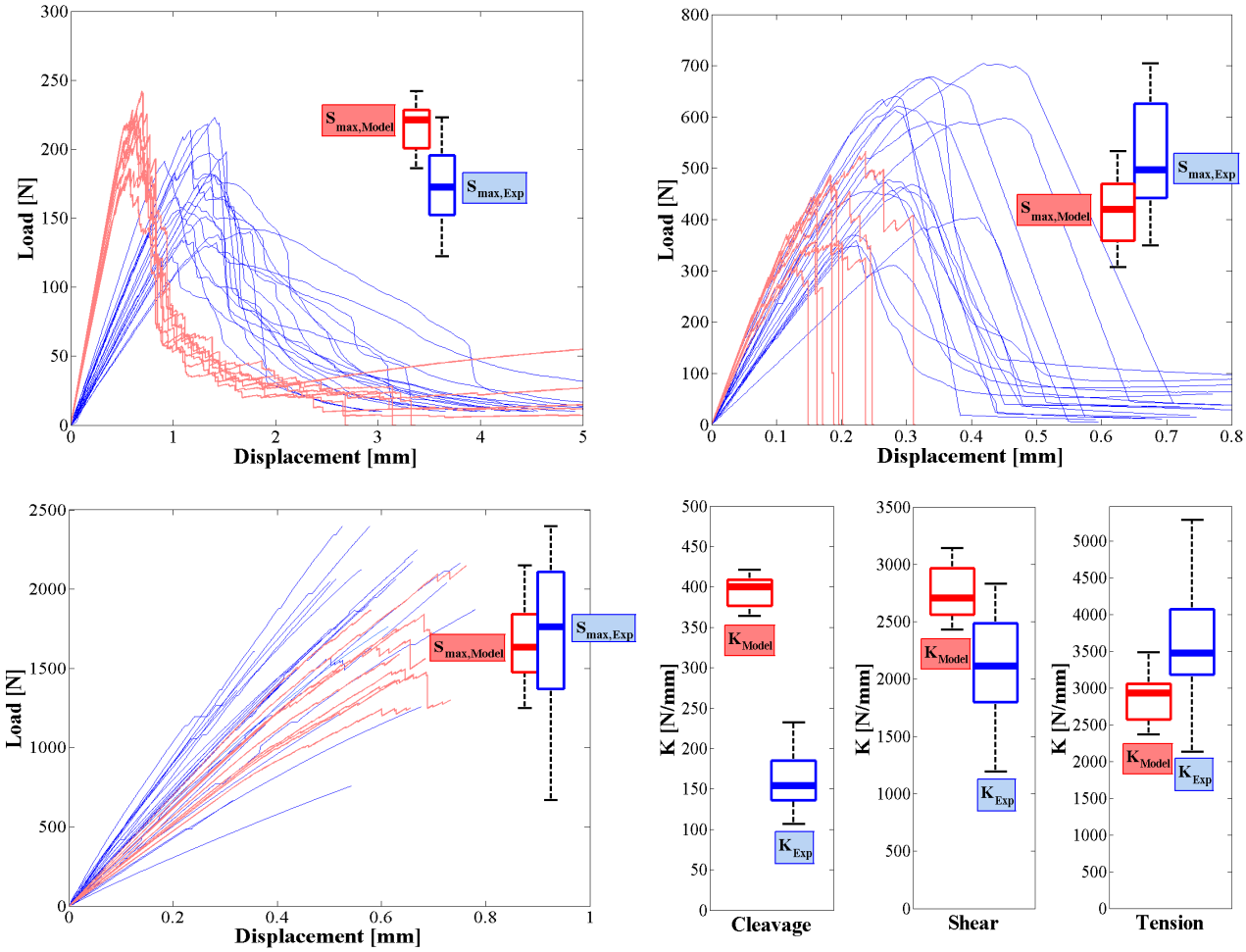

Fig. 8 Load-displacement curves for cleavage, shear and tension tests, box plots show variation in K and S_{max} for model (red) and experiments (blue)

4. Discussion, Conclusions and Acknowledgements

Lattice models seem to be a reasonable approach to model fracture behaviour. Comparisons between experiments and lattice models show that realistic predictions can be made in terms of stiffness, maximum load and fracture path. Heterogeneity was implemented by creating an artificial growth ring structure. This has a significant influence on the fracture path which can be observed in the model as well as in tests (see cleavage model in Fig. 7).

However, since it was important to minimise the computational effort various techniques and approximations were applied. For example, one major drawback is that the lattice does not perfectly represent transverse isotropy (i.e. can not be adjusted freely to any given set of elastic properties). The only solution, to use angular springs, leads to even more strength parameters that need to be determined and to more computation time.

The authors acknowledge the experimental work for measuring density samples taken place in the Agricultural & Analytical Chemistry Department at the University of Glasgow. Furthermore, they want to express their gratitude for the financial support from the Royal Academy of Engineering, Edinburgh, which enabled the participation in the WCTE conference.

5. References

[1] Davids, W. G., Landis, E. N., Vasic, S., "Lattice Models for the Prediction of Load-Induced Failure and Damage in Wood", *Wood Fibre Science*, Vol. 35 PT1, 2003, p.120.

[2] Fournier, C.R., Davids, W.G., Nagy, E., Landis, E.N., "Morphological Lattice Models for the Simulation of Softwood Failure and Fracture", *7th WCCM*, Los Angeles, USA, 2006.

[3] Vasic, S., Smith, I., Landis, E., "Finite Element Techniques and Models for Wood Fracture Mechanics", *Wood Science and Technology,* Vol. 39, 2005, pp. 3-17.

[4] Jirásek, M. and Bažant, Z., "Macroscopic Fracture Characteristics of Random particle Systems", *International Journal of Fracture*, Vol. 69, 1995, pp. 201-228.

[5] Ostoja-Starzewski, M., "Lattice Models in Micromechanics", *Applied Mechanics Reviews*, Vol. 55, No 1, 2002.

[6] Green, D.W., Winandy, J.E. and Kretschmann, D.E.,"Wood Handbook—Wood as an Engineering Material", Chapter 4, *General Technical Report FPL–GTR–113*, Madison, WI: U.S. Department of Agriculture, Forest Service, Forest Products Laboratory, 1999, p. 463.

[7] McLean, J.P., "Wood Properties of four Genotypes of Sitka Spruce", *PhD Thesis*, University of Glasgow, Chemistry Department, 2007.

Nomenclature

α	angle between Y-axis and vector from lattice centre to pith	[rad]
σ, ε, C	stress, strain and elasticity tensor	[N/mm², -, N/mm²]
$\bar{\rho}(r)$	normalised density at radial distance r	[-]
$\bar{\rho}_{diff,i}$	difference between max normalised density and min for ring i	[-]
$\bar{\rho}_{\exp,i}$	exponent parameter in approximated, normalised density function for ring i	[-]
$\bar{\rho}_{min,i}$	minimum parameter in approximated, normalised density function for ring i	[-]
ν_{xy}	Poisson ratio (load applied in X and displacement in Y)	[-]
$\gamma_{C,x,i}$	parameters defining compression softening curve for spring i in X	[-]
φ	probability density	[-]
σ, μ, c_v	mean value, standard deviation, coefficient of variation (σ/μ)	[N, N/mm,-]
dx	lattice spacing in X	[mm]
E_x, G_{xy}	E-modulus in X, shear modulus in XY-plane	[N/mm², N/mm²]
F	force in one spring	[N]
i,j,k,m	arbitrary variables	[-]
K_{Test},K_{model}	overall stiffness for test and model	[N/mm, N/mm]
K_x	mean stiffness parameter in X	[N/mm]
$K_{x,i}$	stiffness parameter in X for spring i	[N/mm]
$l^{(b)}$	length of vector $n^{(b)}$	[mm]
$n^{(b)}$	normalised vector of spring (b) in unit cell	[-]
N_b	number of half springs in one unit cell (18)	[-]
$P_{c,i}$	vector from pith to spring i	[-]
r, r_i, Δr_i	radial distance from pith, radius of ring i, ring width of ring i	[mm, mm, mm]
$\Delta r_{diff,i}$	difference between ring width of ring i and ring i-1	[mm]
r_{pith}	distance from lattice centre to pith	[mm]
$\bar{r}_{shift}$	parameter defining position of specimen in centre growth ring	[-]
r_{var}	difference between radius of ring i, front and backside	[mm]
$S_{C,x,i}$	individual strength parameter for tension in X for spring i	[N]
$S_{T,x}$	mean strength parameter for compression in X	[N]
$S_{max,test/model}$	maximum load for tests and model	[N]
u	displacement in one spring	[mm]
U	strain energy	[N/mm²]
V	volume of lattice unit cell	[mm³]